

Ferrofluid Applications in Chemical Engineering

INVITED PAPER

Pouya Hajiani, Faïçal Larachi

Abstract – Ferrofluids have been vastly wooed in diverse areas of engineering and research. This contribution briefly exposes some concepts specific to ferrofluids and how they relate to recent applications emerging in chemical engineering, including mass transfer enhancement, momentum transfer in laminar and turbulent pipe flows and in porous media flows, and the motion of magnetic nanoparticles in gas-liquid mass transfer mechanisms with/without external magnetic fields. The noticeable effects of magnetic fields on ferrofluid flow behavior will be surveyed as well as a discussion about common assumptions to simplify and solve some ferrohydrodynamic models. With respect to the intriguing features caused by dispersed magnetic nanoparticles on ferrofluid behavior, considerable theoretical and experimental work is left for mining new opportunities in chemical engineering on the subject of ferrofluid interactions between magnetic fields, mass, heat, and momentum transfer phenomena. **Copyright © 2009 Praise Worthy Prize S.r.l. - All rights reserved.**

Keywords: Ferrofluid, Laminar and Turbulent Flow, Porous Media, Mass Transfer Enhancement

Nomenclature

a	Specific interfacial area, 1/m	k_n	Rate constant of nth-order reaction, $\text{m}^3/(\text{mol s})$ for $n = 2$
\mathbf{B}	Magnetic induction vector, T, N/Am	L	Langevin magnetization function operator
C_i^*	Concentration of component i in saturated liquid, mol/m^3	L_{PB}	Column length, m
D	Column diameter, m	L_{tube}	Tube length, m
d	Grain diameter, m	\mathbf{M}	Magnetization vector, A/m
d_{H}	Nanocluster hydrodynamic diameter, m	M_s	Ferrofluid saturation magnetization of the liquid, A/m or Oe
d_{h}	MNP hydrodynamic diameter, m	\mathbf{M}_0	Equilibrium magnetization, A/m
d_{p}	MNP core diameter, m	M'	Magnetization fluctuating component, A/m
d_{tube}	Tube diameter, m	$\sqrt{M_i'^2}$	Magnetization x-component RMS, A/m
E	Absolute enhancement in k_L	m_p	Magnetic dipole moment of single domain nanoparticles, Am^2
E_a	Absolute enhancement in interfacial area	n	Reaction order
E_r	Turbulent rotational kinetic energy, J	Na	Absorption rate, $\text{mol}/(\text{m}^2\text{s})$
E_t	Turbulent translational kinetic energy, J	p	Hydrodynamic pressure, Psi
E'	Absolute enhancement in $k_L a$	Q	Liquid volumetric flow rate, mL/min
f_0	Larmor frequency of magnetization vector in the anisotropy field of the particle, 1/s	r	Radial coordinate in cylindrical coordinate, m
\mathbf{g}	Gravity vector, m/s^2	R	Tube diameter, m
\mathbf{H}	Total magnetic field vector, A/m	Re	Reynolds number
$\mathbf{H}_e, \mathbf{H}_{\text{eq}}$	Effect magnetic field in equilibrium with dynamic magnetization, A/m	rd	Radian
\mathbf{H}'	Fluctuating component of magnetic field caused by turbulence, A/m	T	Absolute temperature, K
I	Moment of inertia per unit mass of MNPs, m^2	T_0	Time-averaged magnetic body couple density, dimensionless
K	Anisotropic constant of material, J/m^3	t	Time, s
k	Turbulent kinetic energy, $\text{kg m}^2/\text{s}^2 = \text{J}$	U	Normalized linear velocity, m/s
k_B	Boltzmann's constant, J/K	U_{int}	Internal energy, J
k_L	Liquid phase mass transfer coefficient, m/s	\mathbf{u}	Ferrofluid linear velocity, m/s
$k_L a$	Volumetric mass transfer coefficient, 1/s	u_{RMS}	Root-mean-square translational velocity, m/s
		u'	Linear velocity fluctuating component, m/s

$\langle u \rangle$	Time averaged linear velocity, m/s
$\sqrt{\overline{u_i^2}}$	Linear velocity x -component RMS, m/s
V_h	MNP hydrodynamic volume, m^3
V_p	MNP core volume, m^3
V_s	Superficial velocity, cm/min
<i>Greek letters</i>	
α	Dimensionless Langevin module
α_{GP}	Gradient programming of the applied magnetic field, A/m^2
ΔP	Pressure drop, Pa
$\Delta \eta$	Rotational viscosity, Pa s
ε	Turbulent kinetic energy dissipation rate, $kg\ m^2/s^3 = J/s$
ε_A	Vortex viscose dissipation rate, cm^2/s^3
ε_C	Rotational kinetic dissipation rate, cm^2/s^3
ε_v	Classical viscous dissipation rate, cm^2/s^3
ζ	Vortex viscosity, Pa s
η'	Shear spin viscosity, kg m/s
θ	The angle between \mathbf{M} and \mathbf{H} , rad
λ	Dilatational viscosity, Pa s
λ'	Bulk spin viscosity, kg m/s
μ	Dynamic viscosity (shear viscosity), Pa s
μ_0	Vacuum permeability $4\pi \times 10^{-7}$, N/A^2 , Tm/A , J/A^2m
ξ	Dimensionless magnetic field
ξ_e	Dimensionless effective magnetic field
ρ	Fluid density, kg/m^3
τ	(Effective) magnetization relaxation time constant, s
τ_{AC}	AC magnetic field oscillation time scale = $1/\Omega_{AC}$, s
τ_B	Brownian relaxation time constant, s
τ_m	Experiment time scale, s
τ_N	Néelian relaxation time constant, s
φ	MNPs' grains volume fraction in colloidal fluid
Φ_b	Energy transfers between translational and rotational kinetic energy, cm^2/s^3
χ_0	Initial magnetic susceptibility,
Ψ	Energy transfers to translational kinetic energy by magnetic field, cm^2/s^3
Ψ_s	Energy transfers to rotational kinetic energy by magnetic field, cm^2/s^3
Ω_{AC}	Oscillating field frequency, Hz
ω	Spin velocity per unit volume of ferrofluid, rad/s Or cm/s
ω'	Linear velocity fluctuating component, m/s
$\sqrt{\overline{\omega_i^2}}$	Spin velocity x -component RMS, rad/s
<i>Subscripts</i>	
i	i direction component of a vectorial field, $i = (x,y,z)$ or (r,θ,z)
L	Liquid phase
MNP	In presence of MNPs
<i>Acronyms</i>	
DLS	Dynamic Light Scattering
fPd	Fractional Pressure Drop

MNP	Magnetic Nanoparticle
PSD	Particle Size Distribution
$p.u.v.$	Per unit volume
RHS	Right hand side
RMS	Root mean square
$rdMNP$	Rigid Dipole Magnetic Nanoparticle
$sdMNP$	Soft Dipole Magnetic Nanoparticle

I. Introduction

Ferrofluids are man-made magnetic colloidal dispersions involving aqueous or organic non-magnetic liquid carriers wherein a large number (*ca.* 10^{17} particles per cubic centimeter) of magnetic nanoparticles (MNP), *ca.* 10 to 15 nm in magnetic core size, are seeded and maintained afloat thanks to thermal agitation and *ad hoc* grafted surfacting moieties [1], [2]. While Brownian agitation prevents MNP sedimentation and, to some extent, magnetic dipole-dipole induced agglomeration, it is insufficient to undo agglomeration by the short-range van der Waals attraction, thus requiring surfactant agents and/or the nanoparticles to be electrically charged to achieve stability of the colloidal system. The giant magnetic moment borne in those MNP inclusions typically ranges between 10^3 and 10^5 Bohr magneton units depending on the (ferri)/ferromagnetic material and particle size [1]. The magnetization of ferrofluids in response to a moderate external magnetic field (about a few tenths of Tesla) is reminiscent of materials endowed with simple paramagnetism; though ferrofluids, in comparison, possess a colossal magnetic susceptibility which is to be linked to the super-paramagnetism stemming from the single-domain feature of their MNPs.

Application of an external magnetic field bestows on ferrofluids unique and intriguing characteristics owing to which they are increasingly scrutinized in the scientific and technical literature. Shifting from the traditional realm of physics to that of engineering at large, ferrofluid applications, in chemical engineering in particular, are perhaps lagging behind those in other engineering areas, as few applications have hitherto been dubbed to chemical engineering. This brief review will be devoted to a discussion of some nascent and potentially relevant applications of ferrofluids to chemical engineering.

We will briefly remind some fundamental concepts of ferrofluids before summarizing the experimental and theoretical studies about mass transfer enhancement, and momentum transfer in laminar/turbulent pipe flows as well as flow through porous media.

II. Background

II.1 Response to Magnetic Field

There are two types of MNPs as regards to freedom of rotation of the magnetic moment vector inside their solid crystal structures. In particles with 'rigid dipoles' (rdMNP) [3], or synonymously 'freezing-in magnetic

moment' [4], the strong anisotropic energy locks the magnetic moment inside the solid crystal. Conversely, 'soft dipoles' particles (sdMNP) enable the magnetic moment to twist freely inside the solid crystal due to thermal agitation perturbations, and therefore exhibit super-paramagnetism [5]. The magnetic dipole moment for each nanoparticle experiences a torque from the magnetic field prevailing inside the ferrofluid which tends to align the magnetic moment to the field direction. In the case of rdMNP, the torque is also felt through the solid body and may result in an "asynchronous" angular motion vis-à-vis the surrounding fluid.

Whereas in the case of sdMNP, alignment of the magnetic moment does not require an exerting torque on the particle's body.

The rdMNP spin can even be blocked, regardless of fluid flow vorticity, if a sufficiently strong *stationary* magnetic field is applied; whilst, in the same conditions, the sdMNP spin would match flow vorticity [3].

Magnetic dipole rigidity or softness is characterized by a relaxation time constant, τ , to be explained later after introducing the magnetization phenomenon.

II.2 Equilibrium Magnetization

Magnetization is the macroscopic magnetic response of a (magnetic or non-magnetic) material to an external magnetic field.

In (motionless) magnetohydrostatic context, the magnetization of ferrofluids is described by means of the same Langevin magnetization equation originally proposed for non-magnetic materials featuring simple paramagnetism [1], [2]:

$$\mathbf{M}_0 = M_s L(\alpha) \frac{\mathbf{H}}{H}, \quad L(\alpha) = \coth(\alpha) - \alpha^{-1}, \quad (1)$$

$$\alpha = \mu_0 m_p H / k_B T, \quad H = |\mathbf{H}|$$

In Eq. (1), m_p is the magnetic dipole moment of one single MNP with magnetic core diameter d_p ; M_s stands for the saturation magnetization which occurs when all the MNP magnetic moment vectors are aligned with the external vector field, H ; μ_0 and k_B are the vacuum permeability and the Boltzmann constant, respectively; and T is the absolute temperature.

II.3 Relaxation Time

Consider an external magnetic field is applied on a collection of MNPs, seeded in a ferrofluid at rest, such that saturation magnetization, M_s , is achieved. After this magnetic field is suddenly disabled, magnetization will decay according to [5]:

$$\mathbf{M} = \mathbf{M}_s e^{-t/\tau} \quad 0 < t < \tau_m \quad (2)$$

where τ_m is the observational time scale of the

experiment and τ is a relaxation time constant. For $\tau_m \ll \tau$, the instantaneous magnetization remains stable near M_s over τ_m . For small τ ($\tau_m \gg \tau$), the instantaneous magnetization decays to zero as time evolves because of the randomizing effect by thermal agitation on the magnetic moments [5]. Thermal agitation in ferrofluids shuffles the magnetic moments following two different mechanisms depending on whether MNPs are rigid or soft dipoles. rdMNPs are randomly, but "bodily", rotated as a result of Brownian collisions. Such a Brownian relaxation mechanism, stemming from a hydrodynamically-driven Brownian rotational diffusion, is characterized by a time constant τ_B [2]:

$$\tau_B = 3V_h \mu / k_B T \quad (3)$$

Martsenyuk et al. [6] attempted to quantify the effect of magnetic field on τ_B using an effective-field theory and the Fokker-Planck equation. They assumed small deviations of magnetization from equilibrium-state magnetization (1) and derived two time constants for relaxation of the parallel and perpendicular (with respect to external magnetic field) magnetization vector components.

They finally concluded that the effect of magnetic field on parallel Brownian relaxation time constant is insignificant, unlike the perpendicular one which is field dependent:

$$\tau_{B\parallel} = \tau_B \quad \tau_{B\perp} = \frac{2\tau_B}{2 + \alpha L(\alpha)} \quad (4)$$

However, a field-invariant τ_B , as calculated from Eq. (3), has been indistinguishably employed in the literature for any magnetic field changes and without verifying Martsenyuk et al. [6] assumptions.

The second thermal agitation mechanism of magnetization relaxation manifests due to rotation of the magnetic moment inside the crystal lattice of the particle and does not necessitate "bodily" rotation of the MNP, *per se*. This mechanism applies to sdMNP and is characterized by a Néelian relaxation time constant, τ_N [1], [2]:

$$\tau_N = \frac{1}{f_0} \exp\left(\frac{KV_p}{k_B T}\right) \quad (5)$$

MNP size distributions in commercial ferrofluids present some polydispersity so that soft and rigid dipoles may coexist within the same fluid sample with a threshold size demarcating the finer sdMNP, which relax according to a Néelian mechanism, and coarser rdMNP which swerve following a Brownian mechanism.

In this case, Martsenyuk et al. [6] proposed to use an effective relaxation time constant defined as a harmonic mean between τ_B or τ_N [1] to reflect more weight by the smaller of the two relaxation times:

$$\tau = \frac{\tau_N \tau_B}{\tau_N + \tau_B} \quad (6)$$

II.4 Magnetization Relaxation Equation

Different dynamic circumstances may arise in practice in which the magnetization vector cannot catch up instantaneously with the equilibrium magnetization vector. These comprise, for instance, ferrofluids subject to time-varying magnetic fields such as rotating or alternating current (AC) magnetic field. In motionless ferrofluids under rotating magnetic fields, the magnetization vector, \mathbf{M} , lags behind the magnetic field vector, \mathbf{H} , due to the relaxation time. In AC magnetic fields, despite \mathbf{M} is all the time collinear with \mathbf{H} , relaxation is also in action due to the distribution in magnetic dipoles misalignments. Another example resulting in a lack of collinearity between \mathbf{M} and \mathbf{H} can also be due to local flow vorticity when a ferrofluid is set to motion in a magnetic field featuring a normal component with respect to the vorticity axis. These cases, or variants thereof, require establishment of a constitutive equation for non-equilibrium magnetization to account for the relaxation phenomenon. Since an accurate and comprehensive kinetic theory to describe MNP relaxation at the microscopic level has yet to be developed, ersatz phenomenological approaches have been considered [7]. Three major magnetization equations have been proposed in the literature which shall be recalled briefly.

Shliomis [8] pioneered the contributions regarding the magnetization relaxation constitutive equations. In his approach, the magnetization relaxation equation treats a ferrofluid as a homogeneous fluid. A slight deviation from equilibrium magnetization of the locally-averaged magnetization, i.e., $1/\tau(\mathbf{M}-\mathbf{M}_0)$, was assumed along with considering the rotation of local magnetization vector coupled to the locally-averaged spin velocity of MNP, $\boldsymbol{\omega}$, i.e., $\boldsymbol{\omega} \times \mathbf{M}$, to account for the exchange to external-observer referential:

$$\frac{\partial \mathbf{M}}{\partial t} = -\mathbf{u} \cdot \nabla \mathbf{M} + \boldsymbol{\omega} \cdot \mathbf{M} - \frac{1}{\tau}(\mathbf{M} - \mathbf{M}_0) \quad (7)$$

where \mathbf{u} is the ferrofluid linear velocity and τ is as defined in Eq. (6).

However, the predictive capability of Eq. (7) was challenged by Bacri et al. [9] as it was found unsuccessful in predictions of experimental results especially for hydrodynamic time scales ($1/|\nabla \times \mathbf{v}|$) smaller than the relaxation time.

In a second approach, Martsenyuk et al. [6] improved the former magnetization relaxation equation by defining a local *effective* magnetic field, \mathbf{H}_e , under which magnetization would follow Langevin equilibrium equation [6]. In doing so, they solved the Fokker-Planck equation on locally averaged (macroscopic) MNP dipole

moment vector distribution, obtaining a dynamic magnetization equation with a set of two time constants [6], [10]:

$$\begin{aligned} \frac{\partial \mathbf{M}}{\partial t} = & -\mathbf{u} \cdot \nabla \mathbf{M} + \left(\frac{1}{2} \nabla \cdot \mathbf{u} \right) \cdot \mathbf{M} - \frac{1}{\tau} \left(1 - \frac{(\boldsymbol{\xi} \cdot \boldsymbol{\xi}_e)}{\xi_e^2} \right) \mathbf{M} + \\ & - \frac{1}{6\mu\phi} \left(\frac{\xi_e - L(\xi_e)}{\xi_e L^2(\xi_e)} \right) \mathbf{M} \cdot (\mathbf{M} \cdot \mathbf{H}) \quad (8) \\ \xi = & \frac{\mu_0 m_p \mathbf{H}}{k_B T} \quad \xi_e = \frac{\mu_0 m_p \mathbf{H}_e}{k_B T} \quad \mathbf{M} = M_s L(\xi_e) \frac{\boldsymbol{\xi}_e}{\xi_e} \end{aligned}$$

where \mathbf{M} is a non-equilibrium magnetization which is in equilibrium with (dimensionless) effective magnetic field $\boldsymbol{\xi}_e$.

Felderhof and Kroh [11] proposed a phenomenological magnetization relaxation equation in the framework of irreversible thermodynamics by deriving an expression for entropy production during dynamic magnetization [11], [12]:

$$\frac{\partial \mathbf{M}}{\partial t} = -\mathbf{u} \cdot \nabla \mathbf{M} + \boldsymbol{\omega} \cdot \mathbf{M} - \frac{\chi_0}{\tau} (\mathbf{H} - \mathbf{H}_{eq}) \quad (9)$$

where χ_0 given as $\lim_{H \rightarrow 0} (M_0/H) = (\mu_0 m_p M_s) / (3k_B T)$ is the initial susceptibility of the ferrofluid obtained in the linear-limit of Langevin function (1). Furthermore, \mathbf{H}_{eq} represents the local equilibrium magnetic field calculated using $\mathbf{H}_{eq} = \mathbf{M}C(|\mathbf{M}|)$. A form of C as used by Schumacher et al. [13] is given as follows:

$$\begin{aligned} |\mathbf{M}| = M_s \left\{ \left(\tanh \left(\frac{3\chi_0}{M_s} |\mathbf{M}| C \right) \right)^{-1} + \right. \\ \left. - \left(\frac{3\chi_0}{M_s} |\mathbf{M}| C \right)^{-1} \right\} \quad (10) \\ |\mathbf{M}| = \sqrt{M_x^2 + M_y^2 + M_z^2} \end{aligned}$$

II.5 Magnetoviscosity

One of the most fascinating attributes of ferrofluids is their ability to exhibit anisotropic apparent viscosity when subject to magnetic fields.

In essence, this anisotropy stems from the rdMNPs being pinned by the magnetic field forcing them to spin asynchronously relative to the contiguous fluid. This leads the wall shear stress a ferrofluid exerts on a wall to change in the presence of a magnetic field [2].

The physical manifestations of this *magnetoviscosity* can be categorized into three classes depending on the nature of the applied magnetic field, i.e., rotating field magnetoviscosity, static (or DC) field magnetoviscosity, and AC field magnetoviscosity. The first type which concerns rotating magnetic fields will not be covered in

this review considering the still remote and irrelevant character of its applications to chemical engineering. However, interested readers can find good accounts on the related physical phenomena in the works of Rosenthal et al. [14], Rinaldi et al. [15], and He et al. [16]. DC-field magnetoviscosity arises when the external field exhibits a perpendicular projection with respect to the fluid vorticity vector, which we refer to as the normal-to-vorticity magnetic field component ($H_{\perp(\nabla \times v)} \neq 0$).

This magnetoviscous behavior was first observed by Rosensweig et al. [17] and McTague [18], and a theoretical framework to explain it was elaborated by Shliomis [18].

While rdMNPs tend to be rotated by fluid vorticity under viscid-flow shear forcing, the normal-to-vorticity magnetic field component hinders the dipoles free rotation.

This results in an inflated apparent viscosity. A directional mismatch between \mathbf{M} and \mathbf{H} occurs in response to an ensemble-average effect of the local fluid's frictional torques exerting on each MNP.

This causes inflation in the measured viscosity denoted, in the literature, as rotational viscosity, $\Delta\eta$ [1], [4].

Fig. 1 depicts a representative rdMNP in planar (Couette or Poiseuille) flow subject to (+ x oriented) static magnetic field as explained by Shliomis [8] and Rosensweig [2].

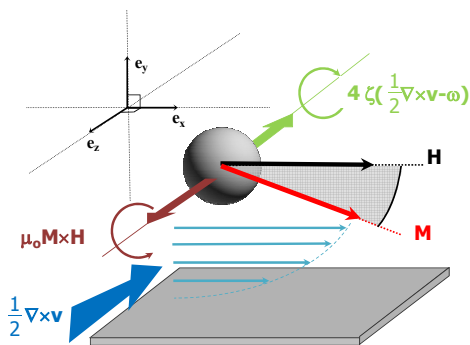


Fig. 1. Steady-state illustration of typical rdMNPs subject to DC magnetic field in planar Couette or Poiseuille flow. Deviation of magnetization from x direction is due to fluid vorticity [2], [8]

It can be seen that the resulting (+ z oriented) magnetic torque acts in opposition to the (- z oriented) vorticity torque (i.e., mechanical torque). Obviously, magnetoviscosity would not manifest in ($\pm z$ oriented) magnetic fields as \mathbf{M} would be able to align with \mathbf{H} without being bothered by vorticity. AC-field magnetoviscosity was first theoretically conceived by Shliomis and Morozov [4] and then experimentally investigated by Bacri et al. [9] and Zeuner et al. [19].

Ferrofluids are polarized linearly (i.e., with invariant direction) with an alternating magnetic field (Fig. 2) so that their rdMNPs would try to imitate the \mathbf{H} pattern via gyration.

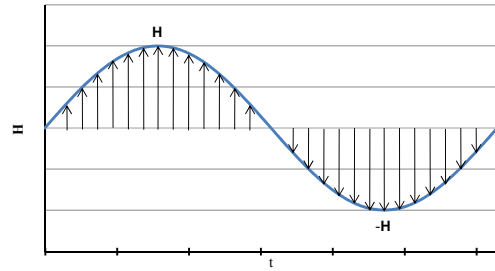


Fig. 2. One cycle of AC-field oscillation

In the motionless case, gyration transitions are racemic in the sense that the rdMNPs have two equiprobable choices to swing, either clockwise or anticlockwise, in a manner reminiscent of a metronome rhythm imposed by the alternating magnetic field. This entrains the average spin angular velocity per unit volume (p.u.v.) of ferrofluid to be in permanence zero, i.e., $\omega = 0$, with \mathbf{M} being forced to transition across 0 in its quest in tracking \mathbf{H} . In shear flows and provided ($H_{\perp(\nabla \times v)} \neq 0$), the rdMNP spin is partly orchestrated by the fluid vorticity which imposes its rotational direction, $\nabla \times v$, as the preferential direction. This biasing direction destroys symmetry between the two aforementioned equiprobable swing directions by privileging the one as illustrated in Fig. 3 and 4.

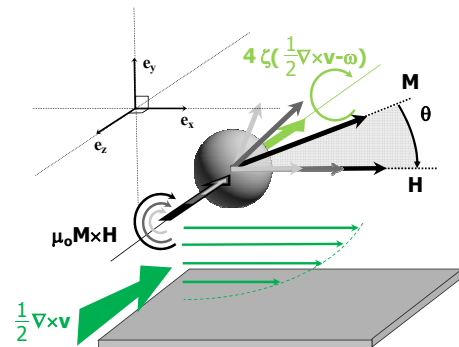


Fig. 3. Schematic of MNPs exposed to AC magnetic field in plane Couette or Poiseuille flow in rising part of the cycle. Deviation of magnetization from x direction is caused by fluid vorticity [4]

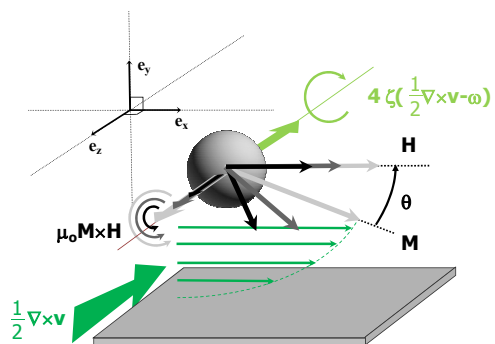


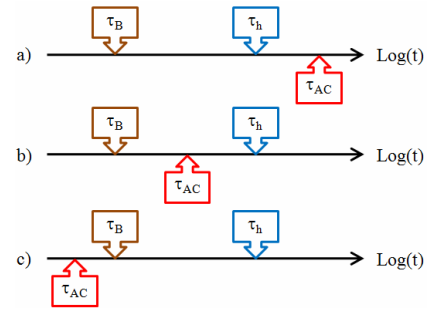
Fig. 4. Schematic of MNPs exposed to AC magnetic field in plane Couette or Poiseuille flow in diving part of the cycle. Deviation of magnetization from x direction is caused by fluid vorticity [4]

Fig. 3 depicts the rdMNP behavior of a Couette-Poiseuille flow in an AC magnetic field while the field is rising to maximum amplitude, and conversely Fig. 4, while the field is decreasing to zero [4]. Shliomis and Morozov [4] view the “vorticity” slap on the rdMNP as the determining event for the initialization of rotation of the magnetization vector [in its quest for catching up the varying magnetic field]. We will denote the fluid vorticity (hydrodynamic) time scale as τ_h . They also view the characteristic time scale of AC magnetic field as equal to the Brownian relaxation time τ_B that is the characteristic time for which the magnetization vector is locked to the changing magnetic field. Assuming $Re \approx 1$, they arrived at $\tau_B \ll \tau_h$ which implies that the rotation of \mathbf{M} , after its initiation by the vorticity slap, is relayed by the AC magnetic field. This nuances the role of fluid vorticity in the rotation of the rdMNPs as it only comes into play as a starter, each time \mathbf{H} transitions through $\mathbf{0}$ (Fig. 2). It has been shown theoretically [4] and later proven experimentally [9], [19] that low frequency ($\Omega_{AC}, \Omega_{AC}\tau_B < 1$) AC field inflates ferrofluid apparent viscosity, that is $\Delta\eta > 0$ and $\omega < \frac{1}{2}|\nabla \times \mathbf{v}|$. When $\Omega_{AC}\tau_B = 1$, the magnetoviscous effect is nullified ($\Delta\eta = 0$) which is tantamount to $\boldsymbol{\omega} = \frac{1}{2}\nabla \times \mathbf{v}$ or to cancelled friction torque between rdMNP and fluid mixture. High frequency magnetic fields ($\Omega_{AC}\tau_B > 1$) induce energy transfers from the AC field to the fluid flow *via* rdMNP kinetic energy. It is this “oriented” energy transfer that decreases the apparent viscosity ($\Delta\eta < 0$; $\omega > \frac{1}{2}|\nabla \times \mathbf{v}|$). Unlike what is shown in Fig. 3 and 4, the mechanical torque exerted on the rdMNP is in opposite direction [4]. It is this phenomenon which is referred to as negative rotational viscosity in the literature. We have just seen that three characteristic times come into play in ferrofluid AC-field magnetoviscosity. Figs. 5(a)-(c) highlight the three possible scenarios that might occur depending on the values of τ_B , τ_{AC} ($= 1/\Omega_{AC}$), and τ_h ($= 1/|\nabla \times \mathbf{v}| \approx R/u_{RMS}$). Let us analyze the “rotational” fate of the rdMNP within one AC-field cycle.

For case I ($\tau_B < \tau_h < \tau_{AC}$, Figs. 5(a)), when \mathbf{H} transitions across zero, Brownian agitation is capable of quickly randomizing the rdMNPs orientations because such reshuffling requires less time than the AC-field period. In addition, since $\tau_h < \tau_{AC}$, the breakage (with respect to fluid vorticity) is the most acutely felt by the rotating rdMNP when \mathbf{H} is about to peak twice within each cycle, i.e., at its maximum and minimum values (Fig. 2). This breakage gives rise to positive rotational viscosity ($\Delta\eta > 0$). In case II ($\tau_B < \tau_{AC} < \tau_h$, see Figs. 5(b)), Brownian agitation entails the same effect as in case I. However, remagnetization of the ferrofluid after it is Brownianly reshuffled (near $\mathbf{H} \approx \mathbf{0}$) follows a path similar to the one depicted above in the motionless situation, that is $\omega \approx 0$ when \mathbf{H} is decreasing towards $-\mathbf{H}$. This explains in part the occurrence in case II of $\omega < \frac{1}{2}|\nabla \times \mathbf{v}|$ and of the positive rotational viscosity effect.

In case III ($\tau_{AC} < \tau_B < \tau_h$, see Figs. 5(c)), and unlike cases I and II, ferrofluid magnetization survives when \mathbf{H}

comes across $\mathbf{0}$ because Brownian agitation is too slow to disorganize the rdMNPs.



Figs. 5. Impact on AC-field magnetoviscosity phenomena with respect to the relative order of Brownian, hydrodynamic and AC characteristic times: a) $\tau_B > \tau_h > \tau_{AC}, \Delta\eta > 0$; b) $\tau_B > \tau_{AC} > \tau_h, \Delta\eta > 0$; c) $\tau_{AC} > \tau_B > \tau_h, \Delta\eta < 0$

In addition and unlike in the motionless situation, the vorticity slap is crucial at enabling all the rdMNPs to rotate at diapason to allow a *gyrating* magnetization vector to catch the oscillating magnetic field (Fig. 6). Since rdMNP rotation is locked to the frequency of the magnetic field, and this frequency being faster than fluid vorticity, therefore $\omega > \frac{1}{2}|\nabla \times \mathbf{v}|$ yielding negative rotational viscosity ($\Delta\eta < 0$).

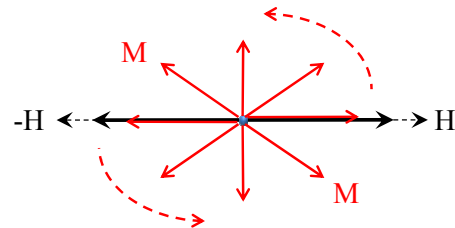


Fig. 6. Oscillating magnetic field causes synchronized rotation of rdMNPs when $\tau_{AC} > \tau_B > \tau_h$

II.6 Ferrohydrodynamic Transport Equations

Solving the ferrohydrodynamic transport equations requires embedding the physical concepts relating to Brownian relaxation, magnetization relaxation, and chiefly, magnetoviscosity, into conventional Newtonian non-magnetic fluid transport equations. This was accomplished by Shliomis [8] as explained in details by Rosensweig [2]. Magnetoviscosity entails the formulation of an internal angular momentum balance equation for the magnetic nanoparticles. The conservation equation of ferrofluid linear momentum writes as:

$$\rho \left(\frac{\partial \mathbf{u}}{\partial t} + \mathbf{u} \cdot \nabla \mathbf{u} \right) = -\nabla p + (\mu + \zeta) \nabla^2 \mathbf{u} + 2\zeta \nabla \cdot \boldsymbol{\omega} + \mu_0 \mathbf{M} \cdot \nabla \mathbf{H} + (\lambda + \mu - \zeta) \nabla (\nabla \cdot \mathbf{u}) \quad (11)$$

Similarly, the conservation equation of ferrofluid

internal angular momentum is:

$$\rho I \left(\frac{\partial \boldsymbol{\omega}}{\partial t} + \mathbf{u} \cdot \nabla \boldsymbol{\omega} \right) = \eta' \nabla^2 \boldsymbol{\omega} + 2\zeta (\nabla \cdot \mathbf{u} - 2\boldsymbol{\omega}) + \mu_0 \mathbf{M} \times \mathbf{H} + (\lambda' + \eta') \nabla (\nabla \cdot \boldsymbol{\omega}) \quad (12)$$

where ρ is the fluid density, I is the moment of inertia per unit mass of MNPs, \mathbf{u} is the linear flow velocity vector, $\boldsymbol{\omega}$ is the spin velocity vector (i.e., average spin rate of all MNPs p.u.v. of ferrofluid [2]), p is hydrodynamic pressure, μ is the dynamic shear viscosity, λ is the dilatational viscosity, η' is the shear spin viscosity, λ' is the bulk spin viscosity, ζ is the vortex viscosity, and μ_0 is the vacuum permeability.

To get a better grasp on understanding Eqs. (11) and (12), it is convenient to recall the physical meaning of each term.

In Eq. (11) RHS aggregates all the terms contributing to the production or consumption of linear momentum for polar fluid endowed with internal angular momentum.

The vortex viscosity increment, ζ , represents the effect of nanoparticles on mixture viscosity, in Newtonian suspension flows, regardless of their magnetic character or application of magnetic field [1], [2]. The next term in Eq. (11) points out that non-uniform spin velocity may induce linear momentum through vortex viscosity.

The Kelvin body force term, $\mu_0 \mathbf{M} \cdot \nabla \mathbf{H}$, stems in situations where a spatially inhomogeneous magnetic field is exerted on incompressible ferrofluids. The last term in Eq. (11) is often dropped for incompressible ferrofluids, which is a common assumption.

The RHS first term in Eq. (12) derived from the divergence of spin gradient tensor stands for spin viscous diffusion between rotating MNP clumps (in the volume average sense) laying in the same neighborhood. The second term represents inter-conversion between internal and external angular momenta.

Fluid vorticity represents the flow tendency to rotate free infinitesimal elements, such as MNP, while $\boldsymbol{\omega}$, the actual MNP spin rate, arises from the magnetic torque felt by the MNP.

As a result, this coupling transfers angular momenta between MNP and ferrofluid. The magnetic body couple density, $\mu_0 \mathbf{M} \times \mathbf{H}$, stands for the magnetic torque exerted on the magnetic particles and driving their rotation. In some specified flow geometries, the MNP spin velocity vector field, appearing in the last term of Eq. (12), is assumed solenoidal [2], [20].

One such a geometry in which $\nabla \cdot \boldsymbol{\omega} = 0$ occurs when the 2nd and 3rd terms of Eq. (12) RHS are collinear with fluid vorticity $\frac{1}{2} \nabla \times \mathbf{u}$ vector as exemplified in Fig. 7 [21], [22], [23]. Fluid vorticity is parallel to y -direction before applying magnetic field as is also the case with $\mu_0 \mathbf{M} \times \mathbf{H}$ when the field is enabled. As a result, $\omega_x = \omega_z = 0$ and ω_y is only x dependent.

The ferrofluid continuity and conservation equations of the linear and internal angular momenta combined with one of the magnetization relaxation equations discussed in section II.5, are in principle closed by adjoining the Maxwell equations.

Maxwell's equations consist of the Gauß's law for magnetic flux density and the (zero free-current density) Ampere's law for magnetic field intensity, respectively:

$$\nabla \cdot \mathbf{B} = 0, \quad \nabla \cdot \mathbf{H} = \mathbf{0} \quad (13)$$

Vector fields \mathbf{B} , \mathbf{H} and \mathbf{M} are related through the well-known BHM constitutive equation:

$$\mathbf{B} = \mu_0 (\mathbf{M} + \mathbf{H}) \quad (14)$$

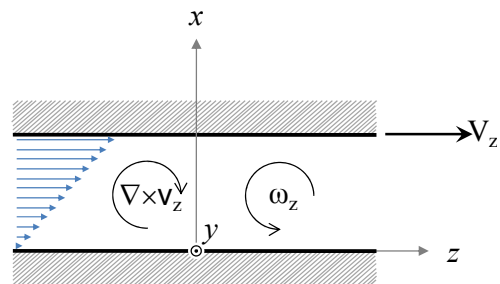


Fig. 7. Couette flows of ferrofluid confined between two parallel plates subject to magnetic field. Adapted from [21]

In Eq. (14), \mathbf{B} and \mathbf{H} are, respectively, *total* magnetic flux density and *total* magnetic field intensity in which both external field and induced field generated by (and felt within) ferrofluid are summed-up. Outside the ferrofluid domain, for instance in the non-magnetic surrounding material, the contribution of magnetization *via* BHM constitutive equation is marginal ($\chi \approx 0$) with \mathbf{B} and \mathbf{H} only generated by the sources external to the non-magnetic material (i.e., including the ferrofluid magnetization contribution).

II.7 Pipe Flow Momentum Transfer

Further than the experiments performed in AC fields by Bacri et al. [9] and Zeuner et al. [19] to validate the magnetoviscosity theory, Schumacher et al. [24] aimed at investigating the effect of AC fields on pressure drop of ferrofluid pipe flow in laminar and turbulent regime. They also proposed a computational model based on ferrohydrodynamic theory and accompanied it with experimental data. Schumacher et al. [24] tested AC (in the [0-1] kHz range) magnetic field in the range [0 - 1264] Oe with a ferrofluid passing through 3 mm inner diameter tube. They defined the fractional pressure drop ($fPd = \Delta P(H)/\Delta P(H = 0) - 1$) merely as the relative variation of (downstream) pressure drop subject to H (inside solenoid) with respect to (upstream) pressure drop (outside solenoid, i.e., $H = 0$) over equal tube lengths and fully developed flows. As illustrated in Fig.

8, fPd was obtained for a range of Reynolds numbers covering laminar and transitional flow regimes. This figure highlights a strong dependence of fPd to flow rate. Based on the arguments discussed above regarding AC-field magnetoviscosity, fPd can take negative values (i.e., negative pressure drop) only if $\Omega_{AC}\tau_B > 1$. The maximum $\Omega_{AC}\tau_B$ reached by Schumacher et al. [24] was 0.061 thus explaining why only $fPd > 0$ were reported coherent with expectation from theory.

In the two sub-sections below we will try to summarize the modeling efforts by these authors regarding the ferrohydrodynamic models in laminar and turbulent pipe flows. TABLE I lists the parameters used by Schumacher et al. [24] in their ferrofluid flow simulations.

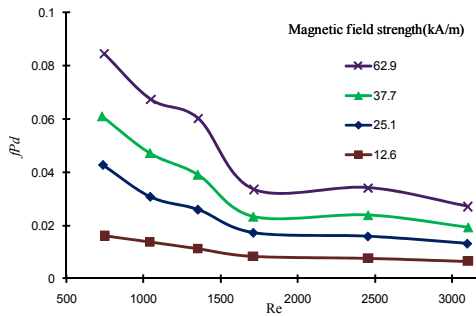


Fig. 8. Fractional pressure drop versus ferrofluid Re measured at different strengths of 400 Hz AC magnetic field. Adapted from [24]

TABLE I
PARAMETERS USED IN FERROFLUID LAMINAR AND TURBULENT SIMULATIONS [24]

	Laminar Flow Model	Turbulent Flow Model
μ (Pa s)	3.85×10^{-3}	3.85×10^{-3}
ρ (kg m ⁻³)	1187.4	1187.4
ζ (Pa·s)	1.93×10^{-3}	1.93×10^{-3}
η' (kg·m·s ⁻¹)	6.40×10^{-20}	6.40×10^{-20}
$C_1 = \zeta/\mu$	0.5	0.5
$C_3 = \eta'/R^2\zeta$	1.5×10^{-11}	1.5×10^{-11}
Q (mL·min ⁻¹)	500	1400
H (Oe)	948	948
Ω (Hz)	60	60
τ_B (μs)	1.5	1.5
χ_0	0.04	0.04
φ	0.025	0.025

II.7.1 Ferrohydrodynamic Laminar Model

Schumacher et al. [24] solved the one-dimensional axisymmetrical laminar version of pipe flow ferrohydrodynamic model in which the continuity, the linear momentum (11), the angular momentum (12), and the magnetization relaxation (7) equations were simplified into a set of four algebraic 2nd-order differential equations for solving the axial ferrofluid velocity component (u), the MNP spin rate ($\omega = \omega_\theta$), the axial pressure gradient ($-dp/dz$) and the magnetic torque density ($\mathbf{M} \times \mathbf{H}$)_θ as a function of pipe radial coordinate, r . The following assumptions were made:

- (Pseudo)-steady-state flow, $\partial/\partial t = 0$;
- Axisymmetry, $\partial/\partial \theta = 0$;

- Fully developed flow for ferrofluid velocity and MNP spin rate, $\partial u/\partial z = 0$, $\partial \omega/\partial z = 0$;
- Ferrofluid flow is incompressible, i.e., $\nabla \cdot \mathbf{u} = 0$, which is also supported by the fully developed flow assumption;
- In the absence of magnetic field, the spin rate vector $\boldsymbol{\omega}$ is in θ direction. According to AC magnetoviscosity theory [4] summarized above, streamwise \mathbf{H} oscillations constrain $\boldsymbol{\omega}$ to keep along θ direction yielding $\nabla \cdot \boldsymbol{\omega} = 0$ (i.e., $\partial \omega/\partial \theta = 0$). This supports the above axisymmetry assumption;
- The spatially uniform magnetic field entrains that $\mathbf{M} \cdot \nabla \mathbf{H} = \mathbf{0}$ in (11);
- Viscous forces are dominant so that inertial effects in (11) are negligible as well as in (12) so that $\rho l(\mathbf{u} \cdot \nabla \boldsymbol{\omega}) = \mathbf{0}$;
- By extension, inertial effects on transporting magnetization are also neglected in (7), $\mathbf{u} \cdot \nabla \mathbf{M} = \mathbf{0}$. This is justified by the fact that in uniform magnetic field, magnetization spatial dependency is only due to velocity field gradient $\nabla \mathbf{u}$ which is perpendicular to \mathbf{u} in the studied geometry.

Therefore, the linear and internal angular momentum balance equations simplify to:

$$\frac{(\mu + \zeta)}{r} \frac{d}{dr} r \frac{du}{dr} + \frac{2\zeta}{r} \frac{d(\omega r)}{dr} - \frac{dp}{dz} = 0 \quad (15)$$

$$\eta' \left(\frac{d^2 \omega}{dr^2} + \frac{1}{r} \frac{d\omega}{dr} + \frac{\omega}{r^2} \right) - 2\zeta \left(\frac{du}{dr} + 2\omega \right) + \left\langle \mu_0 (\mathbf{M} \times \mathbf{H})_\theta \right\rangle_{1/\Omega_{AC}} = 0 \quad (16)$$

Regarding description of the hydrodynamic effects on the magnetization relaxation phenomenon, Schumacher et al. [24] bypassed the necessity to solve the magnetization relaxation equation by averaging the magnetic body couple density over one cycle of the AC field and by including it in the pseudo steady-state angular momentum balance (16).

Following the same assumption, Zahn and Pioch [22] derived an expression for the time-averaged magnetic body couple density for planar Couette flow subject to a rotating magnetic field (Eq. (17)):

$$T_0 \equiv \frac{\left\langle \mu_0 (\mathbf{M} \cdot \mathbf{H})_\theta \right\rangle_{1/\Omega_{AC}}}{\mu_0 H_0^2} = \frac{0.5}{a^2 + b^2} \chi_0 \left[a(e - c) - \chi_0 (ce + df) \right]$$

$$a = (\omega\tau)^2 - (\Omega_{AC}\tau)^2 + 1 + \chi_0, \quad b = \Omega_{AC}\tau(2 + \chi_0)$$

$$c = \omega\tau + 1, \quad d = f = \Omega_{AC}\tau, \quad e = (1 + \chi_0) - \omega\tau$$

Schumacher et al. [24] assumed this expression also

valid in his AC field Poiseuille flow experiments and used it in (16). Schumacher et al. [24] assumed also a rotation of the magnetization vector, in flow conditions, to track the AC magnetic field. Let us evaluate the likelihood of this assumption in the light of the Shliomis and Morozov [4] AC-field magnetoviscosity theory explained in section II.5. In laminar flow for $Re = 1\ 090$, the hydrodynamic time scale is estimated to be $\tau_h = 1.3$ ms, whereas in the transitional flow region for $Re = 4\ 160$ (the highest Re value hit in the authors' tests) $\tau_h = 0.3$ ms. The Brownian time scale estimated by Schumacher et al. [24] was $\tau_B = 1.5$ μ s. For an AC field, $\tau_{AC} = 8.3$ ms, 1.2 ms, 0.5 ms, respectively, for 60 Hz, 400 Hz and 1000 Hz frequencies. According to Figs. 5 taxonomy, a positive rotational magnetoviscosity prevails in Schumacher et al. [24] tests regardless of AC field frequency. In our opinion, this might affect the hypothesis regarding rotation of the magnetization vector because the magnetization vector may decay twice towards zero during one cycle due to Brownian relaxation in the laminar case, and Brownian and fluid vorticity mechanisms in the transitional case. *Stricto sensu*, this entrains that the magnetization vector keeps nearly parallel to the magnetic field thus yielding on the contrary a nearly zero time-averaged magnetic body couple density instead of what is suggested by (17). A *post facto* justification of this interpretation indeed comes out from the authors' own simulations. For example in Fig. 9 (adapted from Fig. 9 in [24]), it is suggested that MNP spin velocity take the same values as (no-magnetic-field) fluid vorticity. However, the radial velocity profiles with and without magnetic field are virtually identical suggesting that fluid vorticity remains nearly indifferent to magnetic field.

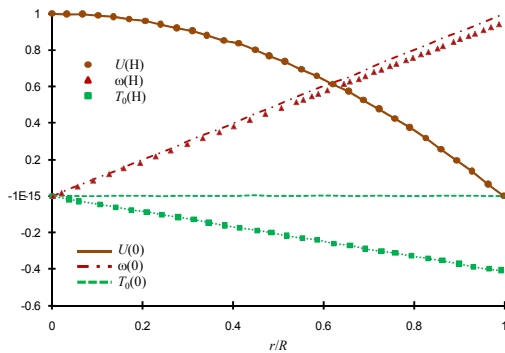


Fig. 9. Simulated profiles of normalized velocity U , spin velocity ω and averaged magnetic body torque T_0 for ferrofluid laminar pipe flow exposed to oscillating magnetic field (948 Oe, 60 Hz) in comparison with zero field profiles. Adapted from [24]

To improve model representation of pressure drop experiments, the authors also assumed an *ad hoc* empirical correction of initial magnetic susceptibility vis-à-vis the applied magnetic field intensity. They also found that τ_B needed to be readjusted in laminar flow regime for each of the AC-field frequencies (Ω_{AC}) and for each flow rate. This further assumption was justified

by the authors as due to the possibility of MNPs agglomeration to form clusters in laminar flow which would imply larger Brownian relaxation time constants instead of the theoretical single MNP (6). Fig. 10 illustrates the fitted cluster Brownian relaxation times normalized by the single MNP τ_B as a function of Re and parameterized by AC field frequency. It can be seen that the higher the Re (similarly, the higher the Ω_{AC}), the lower the τ_B . In the transitional flow regime, the higher shear stresses involved would likely go against cluster formation whereby single MNP τ_B value is sufficient to describe the Re and AC field frequency changes.

Figs. 12(a)-(c) gather the simulated fPD as a function of Re and parameterized with different magnetic field intensities for three different AC field frequencies. The simulated fPD measurements in laminar flow concern the left portion of these figures. It is worthy of notice that the good match between model and measurements is the resultant of the above mentioned two fitted parameters, which indicates that there is still room for developing fully predictive Poiseuille flow models, cfr. Krekhov et al. [25].

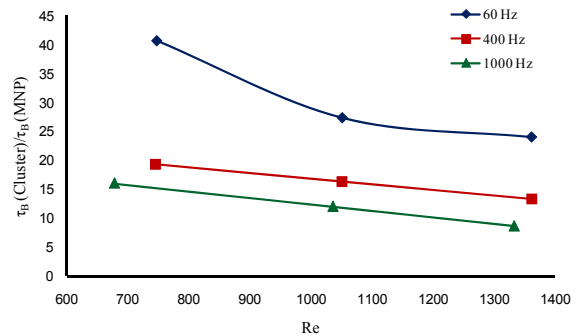


Fig. 10. Fitted Brownian time constant versus ferrofluid Reynolds number at different AC-field frequencies. Adapted from [24]

II.7.2 Ferrohydrodynamic Turbulent Model

The main assumption made by Schumacher et al. [24] is to analogize ferrofluid turbulent behavior to that of a Newtonian fluid suspension with inflated dynamic viscosity, $(\mu + \zeta)$. In their proposed framework, the range of the eddy sizes, from the Kolmogorov length microscale (i.e., smallest eddy size) to the system's integral length scale [26], is not overlapping with the much smaller MNP length scale. Derivation of time-averaged (turbulent flow) forms of ferrofluid linear and angular momentum balance (15) and (16) was attempted.

A low Reynolds number $k-\epsilon$ model was applied to close the Reynolds turbulence stress tensor in the time-averaged linear momentum balance. An important assumption was that magnetoviscosity does not affect turbulent kinetic energy and turbulent kinetic energy dissipation rate [24]. Since time averaging of the angular momentum was taken over one cycle of the AC magnetic field, the averaged angular equation ignored turbulence

connection to spin velocity as if the remote action of magnetic fields on the rotation of the MNPs would remain unfelt at the eddy scale. This is perhaps a gross approximation as is evident from the RHS second term of (12) after introducing the Reynolds decomposition on velocity field, $u = \langle u \rangle + u^*$. In $2\zeta(\nabla \times \mathbf{u} - 2\boldsymbol{\omega})$, MNP spin perturbation originates from two vorticity sources out of the time-average velocity component ($\langle u \rangle$) and the fluctuating velocity component (u^*). Simulations using the low-Reynolds $k-\varepsilon$ turbulence model of the time-average radial profiles of axial velocity component, MNP spin velocity and cycle-averaged magnetic torque density are shown in Fig. 11 for a magnetic field intensity of 948 Oe and AC-field frequency of 60 Hz. Simulations with disabling the magnetic field are also shown for the similar hydrodynamic variables.

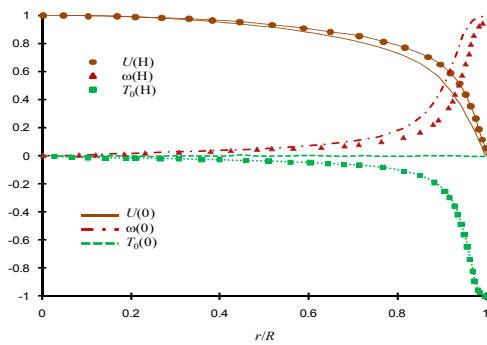
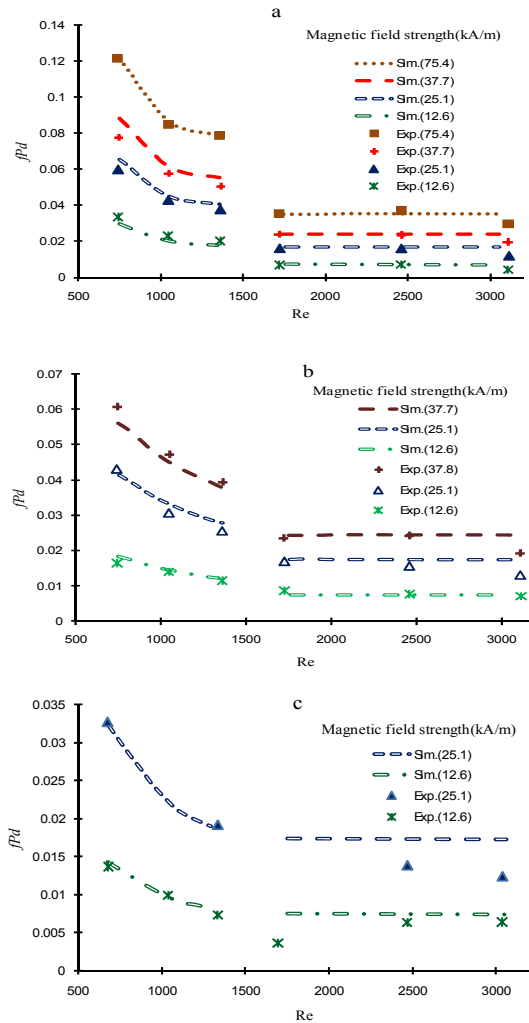


Fig. 11. Simulated profiles of normalized velocity U , spin velocity ω and averaged magnetic body torque T_0 , turbulent kinetic energy k and turbulent dissipation rate ε for ferrofluid turbulent pipe flows exposed to oscillating magnetic field (948 Oe, 60 Hz). Adapted from [24]

Figs. 12(a)-(c) gather the simulated fPd data in the non-laminar region (Figs. 12 right portion) for the same magnetic field features given in the previous section III.1.1. These figures suggest that the simulated fPd are fairly well in agreement in comparison to their measured counterparts. The proposed $k-\varepsilon$ turbulent model represented the fPd experimental data successfully in AC-magnetic fields. Very recently, Schumacher et al. [13] provided a rigorous homogeneous turbulent model for ferrofluid flow subject to steady spatially uniform magnetic field in which flow is simulated in a cube with periodic boundary conditions. An important innovation in their work is the additive inter-conversion of three energy terms representing different forms of energies in ferrofluid including translational kinetic energy $(\rho/2)u_i^2$, rotational kinetic energy $(\rho I/2)\omega_i^2$, and internal energy U .

Time averaging after Reynolds decomposition of the dependent variables, allowed the Reynolds-averaged forms of linear and internal angular momentum and continuity equations to be arrived at. In addition to the classical Reynolds turbulence stress tensor, the averaging procedure brings out three additional nonlinear fluctuating tensors through decomposition of the magnetic field intensity, magnetic flux density and magnetization fields into fluctuating and time average

contributions. These terms are namely the turbulent transport flux of fluctuating spin velocity, the fluctuating Kelvin body force, and the fluctuating body couple density, all of which requiring closures.



Figs. 12. Comparison of simulated Re -dependent fractional pressure drop with experimental data for different oscillating magnetic field strength. Magnetic field frequency (a) 60 Hz, (b) 400 Hz, (c) 1000 Hz. Adapted from [24]

By assuming zero mean velocity and zero spin gradients as well as homogeneous turbulence, to turn to zero all the spatial gradients of averaged quantities, Schumacher et al. [13] proposed expressions for the mean kinetic (translational and rotational) energies and mean internal energy:

$$\begin{aligned} \frac{dE_t}{dt} &= -\varepsilon_V - \varepsilon_A - \Phi_b + \Psi \\ \frac{dE_r}{dt} &= -\varepsilon_C + \Phi_b + \Psi_S \\ \frac{dU_{int}}{dt} &= \varepsilon_V + \varepsilon_A + \varepsilon_C \end{aligned} \quad (18)$$

where:

$$E_t = \frac{1}{2} \rho \overline{u_i'^2}, \quad E_r = \frac{1}{2} \rho I \overline{\omega_i'^2}, \quad U_{int} = \rho \overline{U}_{int}, \quad \varepsilon_v = 2\mu \overline{e'_{ij}e'_{ij}},$$

$$\varepsilon_A = \frac{1}{4\zeta} \overline{A'_i A'_i}, \quad \varepsilon_C = 2\eta' \overline{s'_{ij}s'_{ij}}, \quad \Psi = \overline{u'_i S'_i}, \quad \Phi_b = \overline{\omega'_i A'_i},$$

$$\Psi_s = \overline{\omega'_i Q'_i}$$

where ε_v is the viscous dissipation rate of translational turbulent kinetic energy due to viscous shear stresses, ε_C is the dissipation rate depicting the loss of rotational kinetic energy due to the couple stresses, Φ_b is the rate of work done on the spin by the asymmetric stresses, and results in the transfer of translational kinetic energy to (or from) rotational kinetic energy, ε_A is the dissipation rate of translational kinetic energy due to antisymmetric part of the stress, Ψ is the rate of work done on the turbulent flow by the magnetic body forces, and Ψ_s is the rate of work done on the turbulent flow by the magnetic body couples [13]. These five terms are novelties introduced in this turbulent ferrofluid model. Omitting those degenerates the energy conservation equation to the one as derived for Newtonian fluids.

In their numerical simulations, Schumacher et al. [13] expanded the fluctuating variables as finite three-dimensional Fourier series before performing direct numerical simulation of a ferrohydrodynamic turbulent flow. In the absence of magnetic field, Schumacher et al. [13] showed that ferrofluids behave similarly to a Newtonian fluid. TABLE II lists the magnetic and hydrodynamic properties used in turbulent simulations. Time-average root mean square components of spin velocity and linear velocity are listed in Table II.

TABLE II
MAGNETIC AND HYDRODYNAMIC PARAMETERS
USED IN FERROFLUID TURBULENT SIMULATIONS [13]

d_p (nm)	10
d_h (nm)	29.5
μ (Pa.s)	3.85×10^{-3}
ρ (kg m^{-3})	1187.4
m_p (A m^2)	2.5×10^{-19}
M_s (Oe)	164
ζ/μ	0.5
η' (kg m s^{-1})	2×10^{-15}
τ_B (μs)	10
H (Oe)	158, 316, 1264
χ_0	0.332
T (K)	298.15
d_{tube} (mm)	3
Re	3100
u_{RMS} (cm s^{-1})	20.9

This table indicates that uniform magnetic fields do not affect the RMS fluctuating velocities in turbulent flow simulations. However, there are indications that magnetic fields bring considerable anisotropic dampening in the fluctuations for the two spin velocity components normal to the magnetic field. Induced magnetic field fluctuations and magnetization

fluctuations due to turbulence were also estimated by Schumacher et al. [13] for their particular cubic ferrofluid element.

TABLE III illustrates the marginal contributions of the simulated RMS fluctuating magnetic field and resulting fluctuating magnetization to the applied magnetic field $H = 251 \text{ A cm}^{-1}$ and mean magnetization $M = 68.3 \text{ A cm}^{-1}$. It is worth mentioning that although these fluctuations remain very small in comparison to the mean values, one should be alert that these fluctuations may exhibit non-negligible spatial gradients that could cause significant magnetic body force (via $\nabla \mathbf{H}'$) or magnetic convection (via $\nabla \mathbf{M}'$) terms.

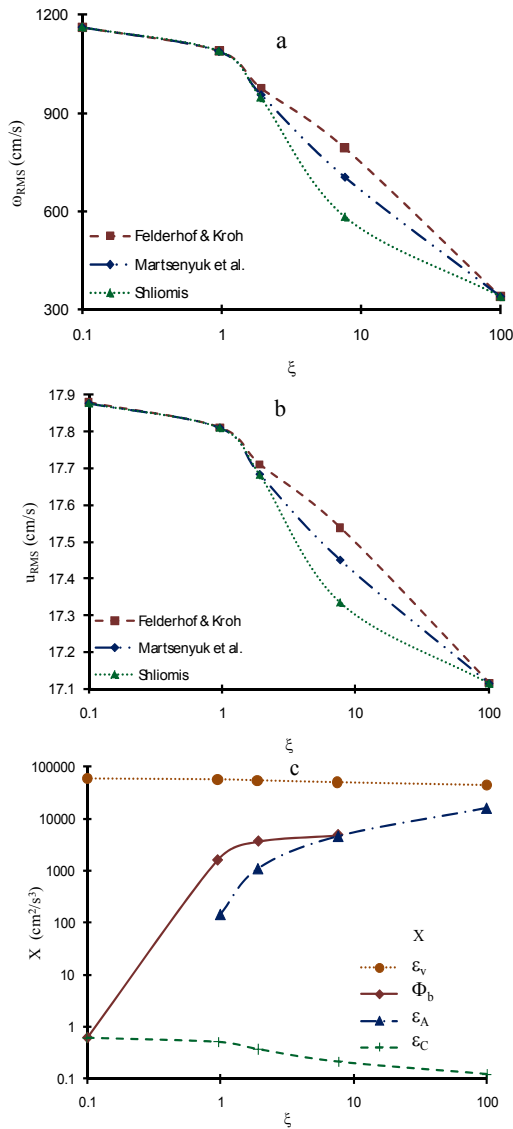
The effect of magnetic field intensity on spin velocity fluctuation and velocity fluctuation is illustrated in Figs. 13(a),(b) as a function of the dimensionless magnetic field (ξ) and using the various most popular magnetization relaxation equations. The damping effect of magnetic field on spin velocity fluctuation is remarkable whereas the velocity fluctuations are barely influenced as already discussed from TABLE III data.

TABLE III
TIME-AVERAGED 3-D SPIN VELOCITY, FERROFLUID VELOCITY,
INDUCED MAGNETIC FIELD AND MAGNETIZATION RMS COMPONENTS
OF TURBULENT FLOW AS SIMULATED IN [13]

H (Oe)	0	158	316	1264
$\sqrt{\omega_x'^2}$ (s^{-1})	379	375	368	355
$\sqrt{\omega_y'^2}$ (s^{-1})	401	364	295	178
$\sqrt{\omega_z'^2}$ (s^{-1})	381	345	280	169
$\sqrt{u_x'^2}$ (cm s^{-1})	19.8	-	19.5	-
$\sqrt{u_y'^2}$ (cm s^{-1})	22.2	-	22.1	-
$\sqrt{u_z'^2}$ (cm s^{-1})	19.6	-	19.4	-
$H = 251 \text{ A cm}^{-1}$				
$\sqrt{H_x'^2}$ (A cm^{-1})	0.049	$\sqrt{M_x'^2}$	0.009	
$\sqrt{H_y'^2}$ (A cm^{-1})	0.062	$\sqrt{M_y'^2}$	0.120	
$\sqrt{H_z'^2}$ (A cm^{-1})	0.069	$\sqrt{M_z'^2}$	0.125	

The effect of magnetic field strength on energetic terms in (18) is illustrated in Figs. 13 using the Shliomis [8] and Martsenyuk et al. [6] magnetization relaxation equations. An instructive display is shown on how energy dissipation terms are mutually involved in

converting energy due to an interacting external magnetic field. The slight decrease of ε_V is very well understood by the fact that the decrease of u_{RMS} versus magnetic field is marginal. The blocking effect of magnetic field on spin velocity fluctuations (Table III, Figs. 13(a)) is mirrored by a reduction in energy dissipation via ε_C . The increasing trend of ε_A as magnetic field is increased can be understood as a hindrance effect by the decreasing spin velocity fluctuations (Figs. 13(b)) on ferrofluid vorticity.



Figs. 13. Effect of magnetic field strength (embedded in dimensionless magnetic field, ξ) on (a) RMS spin velocity, (b) RMS linear velocity, (c) on averaged energy terms: \diamond for Φ_b ; \circ for ε_v ; \square for Ψ_s ; $+$ for ε_C ; ∇ for ε_A , in turbulent model. Adapted from [13]

II.8 Porous Media Momentum Transfer

Taktarov [27], [28] was the first author who considered the motion of magnetizable fluids in porous media. In his study, volume-average formulations of the equations of motion were derived for magnetizable non-

electroconductive liquids in nonmagnetic porous media subject to external non-uniform magnetic fields. Spatial averaging was applied for the linear momentum conservation Eq. (11) assuming zero vortex viscosity ($\zeta = 0$). This led to the neglect in his analysis of formulating an internal angular momentum conservation equation.

More recently, Larachi et al. [29], [30], [31], [32] developed a model of ferrofluid flow through porous media in presence of steady non-uniform magnetic field. The effect of static field magnetoviscosity and magnetic body force on flow behavior was numerically investigated. The starting point of the approach was the microscale ferrohydrodynamic set of ferrofluid phasic equations as depicted in section II.6. Employing spatial averaging theorems, the microscale formulation was muted into macroscale ferrohydrodynamic model equations which led to numerous additional closure terms. Spatially-averaged continuity, linear momentum balance, internal angular momentum balance, and magnetization relaxation equations plus Gauß's law and Ampere's law were obtained for 3-D axisymmetrical cylindrical geometry. The system of partial differential equations was solved for a ferrofluid flow inside packed bed porous media subject to a linearly increasing (or decreasing) external magnetic field in direction of bulk flow (Fig. 14).

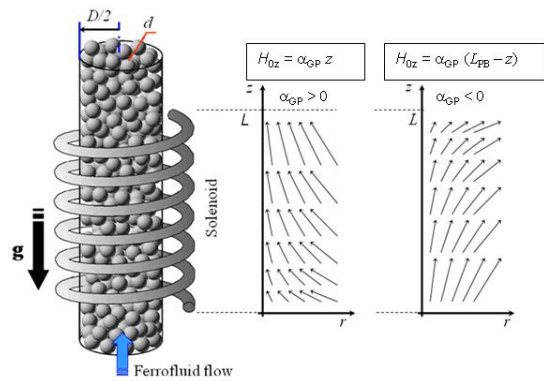


Fig. 14. Porous medium and flow details: Packed bed and magnetic field programming [29]

One application sought out of this work was a magnetic remote control of fluid velocity patterns aimed at overcoming wall channeling and flow short-circuiting in packed beds with low column to particle diameter ratios. As many of the 15 closure terms that arise through volume averaging, some assumptions were made to decouple the ferrohydrodynamic model into a hydrodynamic sub-model and a magnetostatic sub-model. This decoupling was mainly motivated by convergence difficulties associated with induced magnetic field effects. An important result stemming from their simulations was a dramatic reduction of spin velocity due to the external magnetic field close to the packed bed wall (Fig. 15), together with better approach to plug-flow radial velocity profile despite the large permeability contrasts between bed core and wall (Fig.

16). Magnetoviscosity effect was found to prevail mostly close to the wall (Fig. 15).

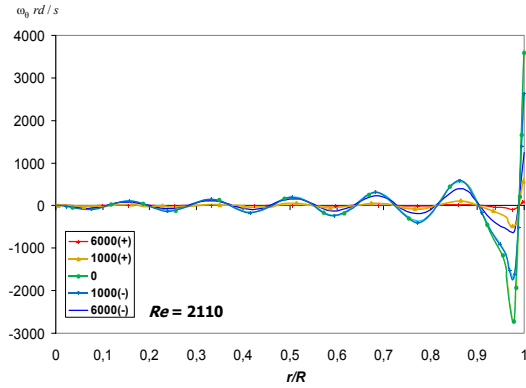


Fig. 15. Spin velocity profiles & positive/negative gradient magnetic field at bed exit $z = L$, $Re = 2110$. Box legend: $A (+) \Rightarrow H_{0z} = A z/L$ Oe; $A (-) \Rightarrow H_{0z} = A (1 - z/L)$ Oe, [29]

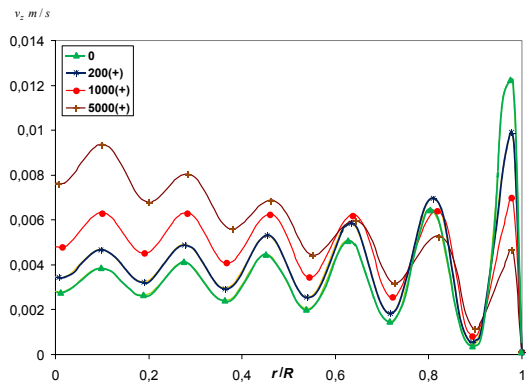


Fig. 16. Axial velocity component radial profiles & positive/negative gradient magnetic field at bed exit $z = L$ and ferrofluid Reynolds numbers $Re = 21.1$. Box legend: $A (+) \Rightarrow H_{0z} = A z/L$ Oe; $A (-) \Rightarrow H_{0z} = A (1 - z/L)$ Oe, [29]

II.9 Mass Transfer Enhancement

Quite recently an emerging trend in chemical engineering concerns attempts to enhance transport operations beyond what can be accomplished in the classical paradigm. For example, it has been stated that the presence of MNPs may enhance gas-liquid mass transfer both in presence and in absence of an external magnetic field.

II.9.1 MNP Suspensions & No Magnetic Field

Olle et al. [33] dispersed MNPs in liquid phase with the objective to enhance gas-liquid mass transfer. The MNPs consisted of oleic-acid grafted surfactant as an internal layer, and (Hitenol-BC) grafted as second-layer polymerizable surfactant. Synthesis, purification and pH stability issues were resolved during the preparation of these MNPs with large hydrodynamic diameter due to the double-surfactant layer. Stability against

agglomeration over a wide pH range was also examined. The volumetric gas-liquid mass transfer coefficient $k_L a$ was determined according to physical and chemical absorption protocols.

During physical absorption, dissolved oxygen absorption dynamic tests were carried out in a flat-surface mechanically-stirred cell. The $k_L a$ values were obtained in the absence of an external magnetic field with and without introducing MNP in the aqueous medium. The MNP mass fractions ranged from zero (control test) to 4%, and an enhancement factor due to the presence of MNPs, was defined as $E_{H=0} = k_{L\oplus MNP}/k_L$. Up to 70% improvement of $E_{H=0}$ is shown in Fig. 17 as a function of stirrer speed and MNP mass fraction. It can be seen that in presence of up to 1% w/w of MNP in liquid, an enhancement of gas-liquid mass transfer takes place. Although the enhancement mechanism is still not elucidated, improvements are more visible at lower agitation rates.

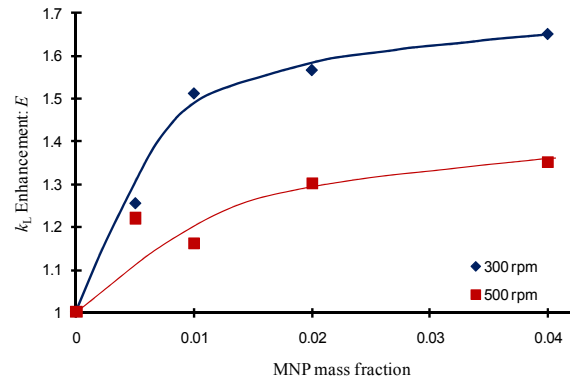


Fig. 17. Enhancement factor vs. MNP mass fraction at 300 and 500 stirrer speed, physical absorption tests. Adapted from [33]

Chemical absorption experiments were also carried out using copper (or cobalt) homogeneously catalyzed oxidation of sulfite into sulfate with dissolved oxygen in aqueous phase.

Copper-catalyzed reaction gave access to the pure physical mass transfer coefficients in the so-called slow-reaction in diffusion film and rapid reaction in liquid bulk (chemical enhancement factor ≈ 1 , O_2 dissolved concentration in liquid bulk ≈ 0). An MNP enhancement factor similar to the one defined in the case of physical absorption was defined while considering that the gas-liquid contacting area is no longer a flat interface:

$$E' = \frac{(k_L a)_{L\oplus MNP}}{k_L a} \quad (19)$$

The cobalt-catalyzed reaction gave access to the gas-liquid interfacial area in the so-called fast-reaction diffusional film (Hatta number > 3 , chemical enhancement factor \approx Hatta number, O_2 dissolved concentration in liquid bulk ≈ 0). An interfacial area

MNP enhancement factor in this absorption regime can be defined as:

$$E_a = \frac{a_{MNP}}{a} = \frac{(Na)_{L\oplus MNP} \left(C_{O_2}^* \sqrt{C_{O_2}^{*n-1}} \right)_L}{(Na)_L \left(C_{O_2}^* \sqrt{C_{O_2}^{*n-1}} \right)_{L\oplus MNP}} \quad (20)$$

Mass transfer coefficient enhancement E' (19) increases with increasing MNP concentration as shown as a function of specific power dissipation and sparging superficial gas velocity and illustrated in Figs. 18 and 19, respectively. The absorption process can be enhanced up to five times due to the presence of MNPs (Fig. 18). However, as power dissipation increases after a certain limit, the enhancement factor decreases, regardless of MNP concentration.

Fig. 19 shows that gas superficial velocity is not a determining operating variable in the enhancement of mass transfer, (20).

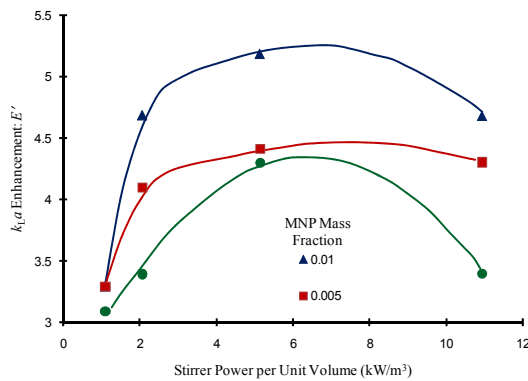


Fig. 18. Enhancement vs. dissipated energy at three different MNP concentrations in chemical absorption tests at $V_s = 14.5$ cm/min. Adapted from [33]

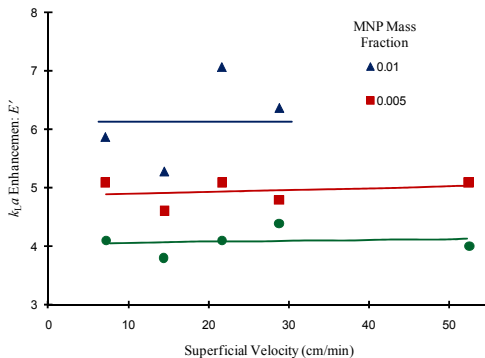


Fig. 19. Enhancement vs. superficial velocity at three MNP mass concentrations in chemical absorption tests at power p.u.v = 2.1 kW/m³. Adapted from [33]

E_a enhancement factor along with E' enhancement factor and the enhancement brought about only on the

pure mass transfer coefficient k_L are illustrated in Fig. 20 and 21. From Fig. 20 it may be seen that most of volumetric mass transfer enhancement is due to the interfacial area growth (more than 80% of 600% total enhancement) over the total range of power draw. The k_L slight enhancement seen at low power input and superficial velocity collapses afterwards when these variables keep increasing. Such effects are coherent with reduction in surface tension with up to 0.1% MNP concentration, as seen commonly during gas sparging in mechanically agitated systems with coalescence inhibiting liquids. However, increasing further MNPs concentration had no major effect on surface tension reduction. These results purport evidence of the presence of MNPs near the gas-liquid interface to explain these enhancement factors. However, no mechanism can be ruled out for explaining the enhancement on k_L and a [33]. The question as to whether this phenomenon is related in any sort to the magnetic nature of nanoparticles has to be elucidated.

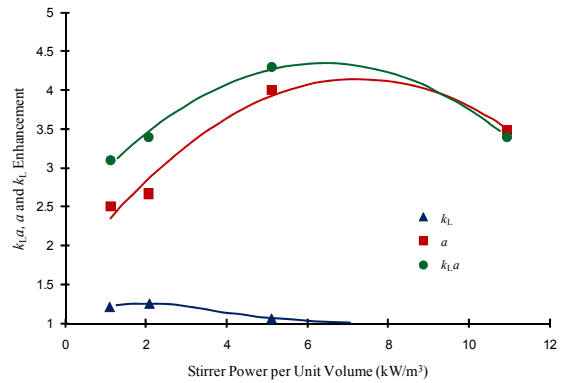


Fig. 20. $K_L a$, a , K_L enhancement vs. dissipated energy at three different MNP concentrations in chemical absorption tests at $V_s = 14.5$ cm/min. Adapted from [33]

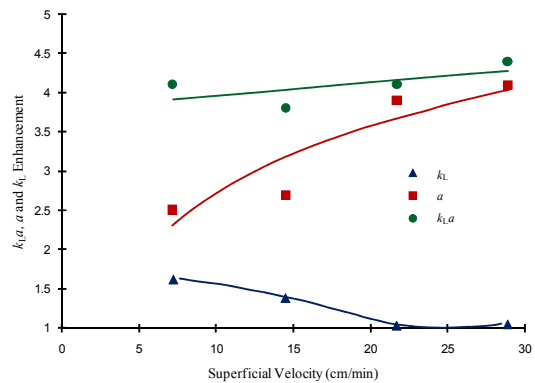


Fig. 21. $K_L a$, a , K_L enhancement vs. superficial velocity at three different MNP concentrations in chemical absorption tests at power p.u.v = 2.1 kW/m³. Adapted from [33]

II.9.2 MNP Suspensions & Magnetic Field

In this approach, first proposed by Suresh and Bhalerao [34], a ferrofluid volume was added to alkaline

aqueous solution in a wetted-wall falling-film column and bubble column to monitor effects from MNP in carbon dioxide absorption using an AC magnetic field to enhance gas-liquid interfacial mass transfer. The Olle et al. [33] measured decrease of surface tension through addition of minor MNP concentration levels indicates that MNP are small enough to protrude through, and populate, the liquid diffusional boundary layer. MNP stimulations by an external magnetic field make them reminiscent of microscale stirrers in the liquid diffusional boundary layer and thus are foreseen to decrease interfacial mass transfer resistance.

A 50-Hz AC magnetic field was generated by two coils one mounted on top of the other. Instantaneous diffusion-limited absorption reactions (CO_2 absorption in carbonate-bicarbonate buffers and in sodium hydroxide solutions) were selected for rate measurements in presence and in absence of AC magnetic field. The saturation magnetization of the ferrofluid used was $M_s = 100$ Gauß before dilution and $M_s = 2$ Gauß after fifty-fold dilution in the alkaline aqueous solutions. Similarly to Olle et al. [33], they reported a slight mass transfer enhancement of ca 5% in the absence of magnetic field and 26% with the magnetic field ON. Since these two studies concerned three different reactor types (falling film, bubble column, stirred tank), apart from the consensual qualitative enhancement in mass transfer, it is difficult to drive the comparisons to a further level.

Mass transfer improvements plateaued after 2.3% v/v MNP ferrofluid was added into the alkaline solutions. Maximum enhancement achieved was 50% on $k_{L,a}$ which is lower than what Olle et al. [33] reported. Possible MNP agglomeration, driven by ionic strength and pH effects, was advanced by the authors as a reason for the lesser improvements arrived at.

More recently, CO_2 absorption was implemented by in methyl-diethanolamine (MDEA) aqueous solutions using a falling-film device [35]. The amine, being tertiary and thus little reactive one, shifts the absorption regime to intermediate between diffusion control and chemical control. A 50% v/v blend of ferrofluid (0.4% solid volume fraction, $M_s = 35$ Gauß) and MDEA solution was used. AC magnetic fields from 100 to 300 Gauß and 500Hz to 100 kHz were tested. Another coil generating up to 1000 Gauß AC field was used to investigate mass transfer enhancement in much stronger fields. Komati and Suresh [35] selected the matrix liquid solution based on MNP size stability. Using a dynamic light scattering technique, ferrofluid colloids were indeed found to be more stable in solutions of tertiary amines, such as triethanolamine and MDEA than ferrofluid in solutions with primary and secondary amines. MNP clusters coarsen in MDEA to a diameter of ca 28-38 nm after ca 5 h and then nearly stabilize in size. Fig. 22 shows the growth of MNP clusters as a function of MDEA concentration and time.

The same enhancement definition (19) proposed by Olle et al. [33] was used by Komati and Suresh [35] and

found that the volumetric mass transfer coefficient can be almost doubled. According to the authors, the flow regime of the falling film precluding ripples' formation on the free surface led them to ascribe the enhancement only to the k_L factor.

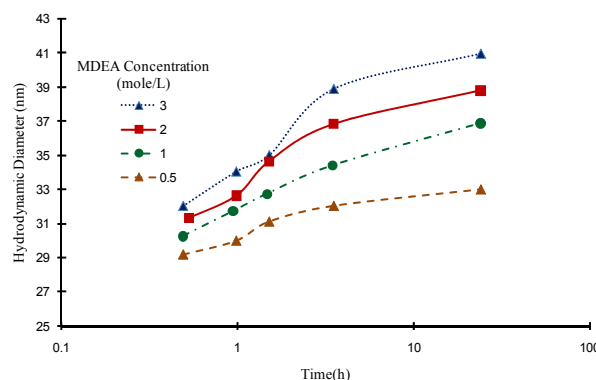


Fig. 22. Stability of magnetic nanoparticle sizes at different concentrations of MDEA vs. time. Adapted from [35]

Most recently, Stuyven et al. [36] devised a clever experiment in which a steady-state homogeneous magnetic field was applied to promote dispersion and disaggregation of non-magnetic nanoclusters in high ionic strength solutions. This approach was dubbed as a new energy process intensification method compared to more conventional disaggregation techniques relying on microwaves, ultrasounds, and jet and ball mills. A mild static magnetic field (0.31 T) was generated by two permanent magnets which set a transverse magnetic field with respect to the flow of silica nanoparticle suspension.

The size of the agglomerated nanoparticles was observed for different Reynolds numbers with and without applied magnetic field. Fig. 23 shows three different particle fraction distributions -PSD- (based on volume). The black line represents PSD in a fluid at rest without external magnetic field. The red line stands for the PSD after 1 h turbulent flow at $Re = 26\ 000$ without external magnetic field.

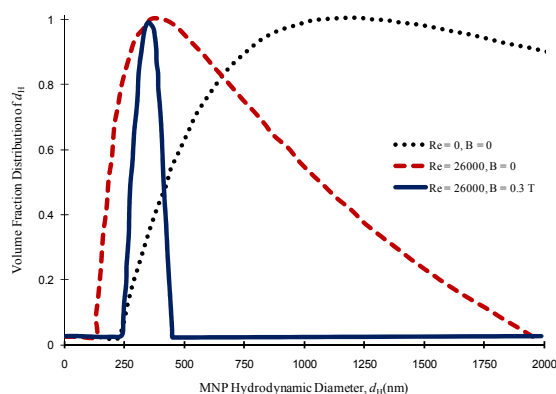


Fig. 23. Particle size distribution of silica aggregates (volume fraction scale), fluid at rest (Black line), after 1 h, $Re = 26\ 000$ in absence (Red line), and in presence (Blue line) of external magnetic field. Adapted from [36]

In this case, the shear forces arising in turbulent flow were able to disaggregate nanoclusters from 1400 nm to 261 nm in size. Applying an external magnetic field at the same Re value reduced further the mean particle diameter to 169 nm (blue line). The narrower PSD shape in this last case indicates that most of the clusters are broken when the Lorentz force come to into play along with the hydrodynamic forces.

Fig. 24 illustrates another experiment by Stuyven et al. [36] in which nanoparticles size stabilized (red portion of the curve on the left) around 390 nm at $Re = 8\ 000$ without magnetic field. Enabling the magnetic field caused a reduction of the mean diameter to 310 nm (blue middle portion) then disabling the magnetic field (red portion of the curve on the right) resumed nearly reversibly re-agglomeration of particles.

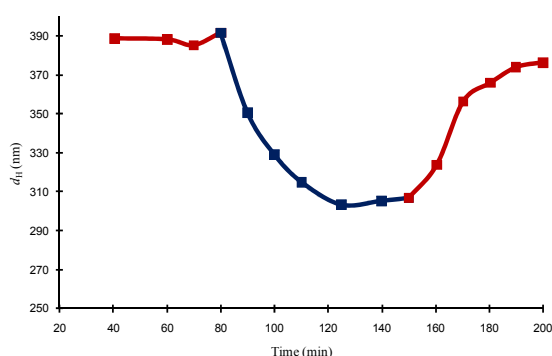


Fig. 24. Particle size evolution of silica aggregates in presence (Blue line) and absence (Red line) of external magnetic field, $Re = 8\ 000$. Adapted from [36]

Another set of experiments was aimed at the study of the effect of Re on the magnetic field-agglomeration interaction. It can be seen that magnetic fields enhance agglomeration in laminar flow regime (Fig. 25) and cluster disaggregation in transitional and turbulent flows.

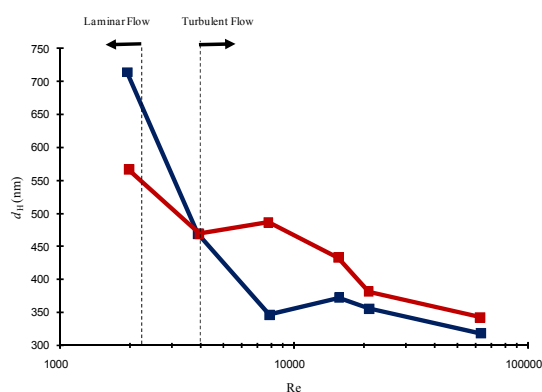


Fig. 25. Mean diameter of γ -alumina clusters formed in presence of magnetic field (Blue line) and in absence of magnetic field (Red line) versus Reynolds number. Adapted from [36]

The stable aggregation was interpreted by Stuyven et al. [36] as resulting from a balance between attractive and repulsive forces between initially charged nanoparticles. In laminar flow, collision frequency is

promoted by the magnetic field while hydrodynamic strain on cluster due to velocity gradient is weak. In this regime the Lorentz force acting on the differently charged nanoparticles, being part and parcel of a given nanoclusters, cannot split them apart, thus agglomeration prevails. Conversely, in turbulent flow regime, the random shear stress fluctuations and strong strain, especially near the wall, promote small size clusters. In this case, the Lorentz force drags the charged clusters towards the wall hence enhancing their disaggregation.

III. Conclusion

In this review, the most relevant theoretical concepts and practical applications of ferrofluid in chemical engineering have been summarized. Although ferrofluids are applied widely across many disciplines and industrial sectors, they have not received sufficient coverage in the realm of chemical engineering. In this brief contribution, some modeling and experimental issues potentially relevant to this area have been discussed. In particular, future research on mass transfer enhancement in the presence of nanoparticles (magnetic or nonmagnetic) and/or magnetic field is foreseen to unveil new mechanisms and discoveries of fluid-fluid enhancement processes of relevance to chemical reaction engineering.

References

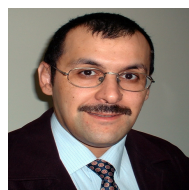
- [1] S. Odenbach, *Magnetoviscous Effects in Ferrofluids* (Springer, 2002).
- [2] R. E. Rosensweig, *Ferrohydrodynamics* (Dover Publications, 1997).
- [3] K. Morozov, M. I. Shliomis, M. Zahn, Magnetoviscosity in suspensions of grains with finite magnetic anisotropy, *Phys. Rev. E* 73 (2006) 066312.
- [4] M. I. Shliomis, K. I. Morozov, Negative viscosity of ferrofluid under alternating magnetic field, *Phys. Fluids* 6 (1994) 2855-2861.
- [5] A. H. Morrish, *Physical Principles of Magnetism* (Wiley Press, 2001).
- [6] M. Martsenyuk, Y. Raikher, M. I. Shliomis, On the kinetics of magnetization of suspensions of ferromagnetic particles, *Sov. Phys. JETP* 38 (1974) 413-416.
- [7] B. U. Felderhof, Flow of a ferrofluid down a tube in an oscillating magnetic field, *Phys. Rev. E* 64 (2001) 021508.
- [8] M. I. Shliomis, Effective viscosity of magnetic suspensions, *Sov. Phys. JETP* 34 (1972) 11291-1294.
- [9] J. -C. Bacri, R. Perzynski, M. I. Shliomis, G. I. Burde, Negative-Viscosity effect in a magnetic field, *Phys. Rev. Lett.* 75 (1995) 2128-2131.
- [10] M. I. Shliomis, Ferrohydrodynamics Testing a third magnetization equation, *Phys. Rev. E* 64 (2001) 060501.
- [11] B. U. Felderhof, H. J. Kroh, Hydrodynamics of magnetic and dielectric fluids in interaction with the electromagnetic field, *J. Chem. Phys.* 110 (1999) 7403-7411.
- [12] B. U. Felderhof, Magnetoviscosity and relaxation in ferrofluids, *Phys. Rev. E* 62 (2000) 3848-3854.
- [13] K. R. Schumacher, J. J. Riley, B. A. Finlayson, Homogeneous turbulence in ferrofluids with a steady magnetic field, *J. Fluid Mech.* 599 (2008) 1-28.
- [14] A. D. Rosenthal, C. Rinaldi, T. Franklin, M. Zahn, Torque measurements in spin-up flow of ferrofluids, *J. Fluids Eng.* 126 (2004) 198-205.
- [15] C. Rinaldi, F. Gutman, X. He, A. D. Rosenthal, M. Zahn, Torque

Authors' information

Chemical Engineering Department,
Laval university,
Quebec,
G1V0A6,
Canada.



Pouya Hajiani (pouya.hajiani.1@ulaval.ca) holds a BS Degree, Major: Chemical engineering, Minor: Petroleum Industry Process Design, University of Tehran (Tehran-Iran), Faculty of engineering, Chemical Engineering Department, 2003. MS Degree, Major: Chemical engineering, Minor: Petroleum Industry Process Design, University of Tehran (Tehran-Iran), Faculty of engineering, Chemical Engineering Department, 2006. He is a PhD candidate in chemical engineering department, Laval University, (Quebec City, CANADA) on the application of Ferrofluids in chemical engineering.



Faiçal Larachi (*Corresponding author: (T)1-418-656-3566; (F)1-418-656-5993; faiçal.larachi@gch.ulaval.ca) is full professor of chemical engineering. He holds a doctoral degree from the *Institut National Polytechnique* de Lorraine in France. His research interests encompass multiphase reactor engineering, chemical kinetics, process intensification, magnetic fields and new approaches for mitigation of greenhouse gas effect. Financial support from the “Chaire de recherche du Canada en procédés et matériaux pour des énergies durables” and the Discovery Grant both from the Natural Sciences and Engineering Research Council (NSERC) is gratefully acknowledged

- measurements on ferrofluid cylinders in rotating magnetic fields, *J. Magn. Mater.* 298 (2005) 307–310.
- [16] X. He, S. Elborai, D. Kim, S. H. Lee, M. Zahn, Effective magnetoviscosity of planar-Couette magnetic fluid flow, *J. Appl. Phys.* 97 (2005) 10Q302.
- [17] R. E. Rosensweig, R. Kaiser, G. Miskolczy, Viscosity of magnetic fluid in a magnetic field, *J. Colloid Interface Sci.* 29 (1969) 680-686.
- [18] J. P. McTague, Magnetoviscosity of magnetic colloids *J. Chem. Phys.* 51 (1969) 133-136.
- [19] A. Zeuner, R. Richter, I. Rehberg, Experiments on negative and positive magnetoviscosity in an alternating magnetic field, *Phys. Rev. E* 58 (1998) 9287-8293.
- [20] C. Rinaldi, A. Chaves, S. Elborai, X. He, M. Zahn, Magnetic fluid rheology and flows, *Curr. Opin. Colloid Interface Sci.* 10 (2005) 141-157.
- [21] M. Zahn, D. R. Greer, Ferrohydrodynamic pumping in spatially uniform sinusoidally time varying magnetic fields, *J. Magn. Mater.* 149 (1995) 165-173.
- [22] M. Zahn, L. L. Pioch, Magnetizable fluid behaviour with effective positive, zero or negative dynamic viscosity, *Indian J. Eng. Mater. Sci.* 5 (1998) 400-410.
- [23] C. Rinaldi, M. Zahn, Effects of spin viscosity on ferrofluid flow profiles in alternating and rotating magnetic fields, *Phys. Fluids* 14 (2002) 2847-2870.
- [24] K. R. Schumacher, I. Sellien, G. S. Knoke, T. Cader, B. A. Finlayson, Experiment and simulation of laminar and turbulent ferrofluid pipe flow in an oscillating magnetic field, *Phys. Rev. E* 67 (2003) 026308.
- [25] A. P. Krekhov, M. I. Shliomis, S. Kamiyama, Ferrofluid pipe flow in an oscillating magnetic field, *Phys. Fluids* 17 (2005) 033105.
- [26] H. Tennekes, J. L. Lumley, *A First Course in Turbulence* (MIT Press, 1972).
- [27] N. G. Taktarov, Motion of magnetizable liquids in porous media, *Magneto-hydrodynamics* 16, (1980) 251-255.
- [28] N. G. Taktarov, Convection of magnetizable fluids in porous media, *Magneto-hydrodynamics* 17, (1981) 333-335.
- [29] F. Larachi, D. Desvigne, Magnetoviscous control of wall channeling in packed beds using magnetic nanoparticles-Volume-average ferrohydrodynamic model and numerical simulations, *Chem. Eng. Sci.* 61 (2006) 1627 – 1657.
- [30] F. Larachi, D. Desvigne, Ferrofluid induced-field effects in inhomogeneous porous media under linear-gradient d.c. magnetic fields, *Chem. Eng. Process.* 46 (2007) 729-735.
- [31] F. Larachi, D. Desvigne, Ferrofluid magnetoviscous control of wall channelling in porous media, *China Particuology* 5 (2007) 50-60.
- [32] F. Larachi, Experimental and theoretical explorations of weak and strong gradient magnetic fields in chemical multiphase processes, Chap. 11 in *Modeling of Process Intensification*, F. J. Keil, (Wiley-VCH, 2007, pp. 365-399).
- [33] B. Olle, S. Bucak, T. C. Holmes, L. Bromberg, T. A. Hatton, D. I. C. Wang, Enhancement of oxygen mass transfer using functionalized magnetic nanoparticles, *Ind. Eng. Chem. Res.* 45 (2006) 4355-4363.
- [34] A. K. Suresh, S. Bhalerao, Rate intensification of mass transfer process using ferrofluids, *Indian J. Pure Appl. Phys.* 40 (2001) 172-184.
- [35] S. Komati, A. K. Suresh, CO₂ absorption into amine solutions a novel strategy for intensification based on the addition of ferrofluids, *J. Chem. Technol. Biotechnol.* 83 (2008) 1094-1100.
- [36] B. Stuyven, Q. Chen, W. V. d. Moortel, H. Lipkens, B. Caerts, A. Aerts, L. Giebel, B. V. Eerdenbrugh, P. Augustijns, G. V. d. Mooter, J. V. Humbeeck, J. Vanacken, V. V. Moshchalkov, J. Vermant, J. A. Martens, Magnetic field assisted nanoparticle dispersion, *Chem. Commun.* (2009) 47-49.